

Sub-femtosecond precision measurement of relative X-ray arrival time for free-electron lasers

N. Hartmann^{1,2*}, W. Helm^{1,3}, A. Galler⁴, M. R. Bionta⁵, J. Grünert⁴, S. L. Molodtsov^{4,6}, K. R. Ferguson¹, S. Schorb¹, M. L. Swiggers¹, S. Carron¹, C. Bostedt¹, J.-C. Castagna¹, J. Bozek¹, J. M. Glownia¹, D. J. Kane⁷, A. R. Fry¹, W. E. White¹, C. P. Hauri^{8,9}, T. Feurer² and R. N. Coffee^{1*}

Today's brightest coherent X-ray sources, X-ray free-electron lasers, produce ultrafast X-ray pulses for which full-width at half-maximum durations as short as 3 fs have been measured¹. There has been a marked increase in the popularity of such short pulses now that optical timing techniques have begun to report an X-ray/optical delay below ~10 fs r.m.s. errors. As a result, sub-10 fs optical pulses have been implemented at the Linac Coherent Light Source (LCLS) X-ray beamlines, thus warranting a push to reduce the error in X-ray/optical delay measurements to the 1 fs level. Here, we report a unique two-dimensional spectrogram measurement of the relative X-ray/optical delay. This easily scalable relative delay measurement already surpasses previous techniques by an order of magnitude with its sub-1 fs temporal resolution and opens up the prospect of time-resolved X-ray measurements to the attosecond community.

X-ray free-electron laser (XFEL) facilities are large machines that often preclude active control of the many sources of noise and jitter, such as jitter in the arrival time of X-rays relative to an external phase-locked optical laser^{2–4}. The recently demonstrated accelerator-based technique of transverse streaking of the spent FEL electron bunch⁵ reports the X-ray pulse shape, but not an X-ray/optical relative arrival time. Photo- and Auger electron streaking can in principle record both the temporal shape and the arrival time of X-ray pulses^{6–8}, but solving the ‘time’ and ‘shape’ problems simultaneously requires difficult frequency regimes, and therefore places heavy resolution and collection requirements on electron spectrometers. In contrast, cross-correlation based on X-ray-induced material changes has seen wide success, with simple implementations^{9–13}. The order-of-magnitude gain in temporal resolution that the spectrogram-based technique portends could deliver the temporal zoom factor needed to peer into some of the fastest chemical and material changes^{14,15} that are triggered at XFEL sources of both soft and hard X-ray photons.

The spectrogram approach described here avoids the disadvantages of two commonly used techniques for timing at the Linac Coherent Light Source (LCLS), spatial and spectral encoding of time. Spatial encoding^{4,10–13,16–18} is susceptible to the X-ray mode variations produced by edge diffraction from X-ray optics, while etalon effects and spectral amplitude fluctuations can affect the edge-finding algorithms used for spectral encoding^{9,12,19}. In the two-dimensional spectrogram technique described here, the curvature of the X-ray-induced signal (Fig. 1) is fitted with a low-order

polynomial. This approach is not only insensitive to the diffraction features typical of apertured, slitted or otherwise clipped X-ray or optical beams, but it is also insensitive to the spectral ripples that arise from etalon and modulations caused by the time-dependent refractive index¹⁹. The computational algorithm takes hundreds of individual lineouts from single-shot images through a few hundred fitting cycles. Such an algorithm is inherently parallelizable and thus suitable for on-the-fly jitter measurements.

Spectrogram-based timing resembles the frequency-resolved optical gating (FROG)²⁰ technique that is common for optical pulse characterization. Unlike an instantaneous optical gate, in our case the X-ray-induced carrier dynamics in silicon nitride gate the optical probe with a step-like change in optical absorption and phase. In the carrier gate process, X-rays interact with a material to produce high-energy photoelectrons and core-level holes²¹. The high-energy electrons scatter inelastically with the valence and conduction electrons in the material, and the core-level holes similarly scatter inelastically into the valence band. The result is a cascade of secondary electrons followed by rapid thermalization, which converts the absorbed X-ray dose into few-eV electron-hole excitations^{22,23}. This process takes place on the 1–100 fs timescale, depending on X-ray photon energy and material composition. The electron-hole excitations alter the complex refractive index of the material, modulating the optical reflective and transmissive properties. This change indicates the X-ray pulse arrival time when probed by an optical pulse. We resolve the fast optical changes with a broadband probe with sufficient intensity for single-shot spectrogram measurements. In such a measurement, the X-ray and optical beams are crossed at an angle. As shown in Fig. 1, the position in the spatial beam profile d maps to relative delay τ by the crossing angle α :

$$\tau = \frac{d \sin \alpha}{c} \quad (1)$$

The spectrogram $S(\tau, \tilde{\omega})$ is recorded as a function of the delay and frequency of the probe pulse $E(t)$ (Fig. 1) using an imaging spectrograph and a charge-coupled device (CCD) camera, where

$$S(\tau, \tilde{\omega}) = \left| \int dt E(t) G(t - \tau) \exp(i\tilde{\omega}t) \right|^2 \quad (2)$$

The width of the gating function G depends on the X-ray intensity profile and the material response time. If the response time is much

¹The Linac Coherent Light Source, SLAC National Accelerator Laboratory, 2575 Sand Hill Road, Menlo Park, California 94025, USA, ²Institute of Applied Physics, University of Bern, Sidlerstrasse 5, 3012 Bern, Switzerland, ³Technische Universität München, James-Franck-Strasse 1, 85748 Garching, Germany,

⁴European XFEL GmbH, Notkestrasse 85, 22607 Hamburg, Germany, ⁵LCAR-UMR 5589-Université Paul Sabatier Toulouse III-CNRS, 118 Route de Narbonne, Bat. 3R1B4, 31062 Toulouse Cedex 9, France, ⁶Institute of Experimental Physics, University of Technology Bergakademie Freiberg, Leipziger Strasse 23, 09599 Freiberg, Germany, ⁷Mesa Photonics, LLC, 1550 Pacheco St. Santa Fe, New Mexico 87505, USA, ⁸Paul Scherrer Institute, 5232 Villigen, Switzerland,

⁹Physics Department, Ecole Polytechnique Federale de Lausanne, 1013 Lausanne, Switzerland. *e-mail: hnwick@slac.stanford.edu; coffee@slac.stanford.edu

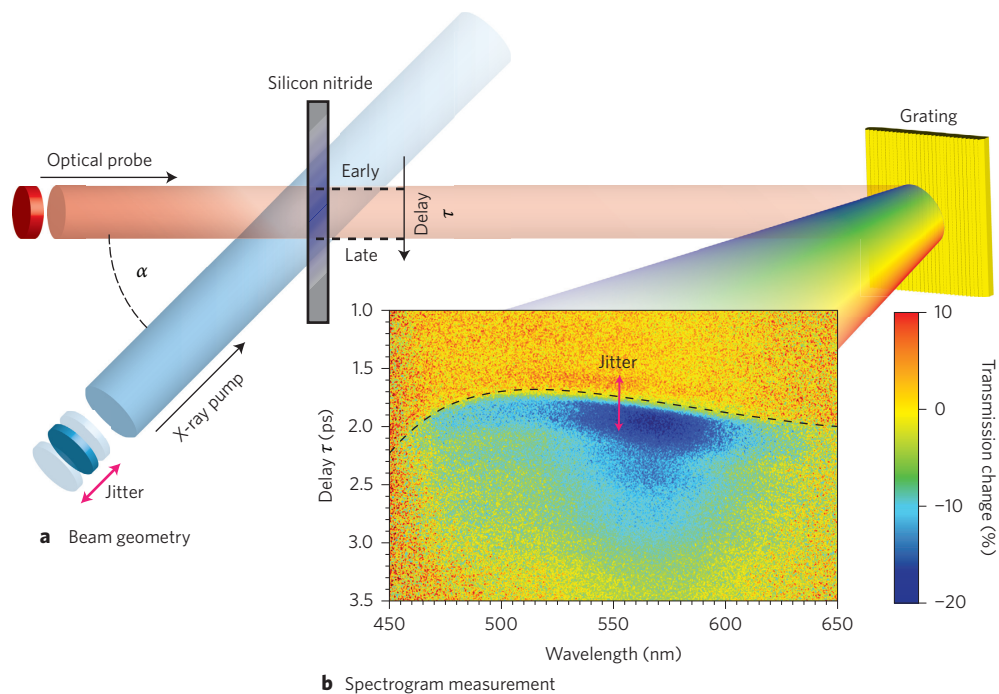


Figure 1 | Schematic of the single-shot geometry for measurement of the spectrogram. **a**, The X-ray and optical beams are crossed in a silicon nitride membrane and their relative delay is encoded in the spatial beam profile of the optical probe. The crossing angle α and beam diameters define the time window in which the X-ray-induced absorption is probed. **b**, Measured spectrogram using an unpumped normalization spectrogram to calculate the change in transmission. The result of the two-step edge-finding algorithm to determine the X-ray arrival time is overlaid as a black dashed line.

longer than the X-ray pulse duration, then any information about the substructure of the X-ray intensity profile is lost during the interaction, and the response function acts like a low-pass Fourier filter. We note that Fig. 6 of ref. 21 indicates a generally shorter material response for lower photon energies. In our case of 800 eV photon energy, ~ 3 fs X-ray pulses and ~ 50 fs material response, the convolution of both is approximated by a Gaussian of width τ_1 . We measure the transmission change ΔT as $S_{\text{sig}}/S_{\text{ref}} - 1$ by using an X-ray pumped spectrogram S_{sig} and an unpumped normalization spectrogram S_{ref} . The observed time-dependent transmission change for a lineout at a given wavelength is baseline corrected and modelled via the maximum transmission change ΔT_{\max} , the effective Gaussian profile centred at time t_0 with width τ_1 , and an exponential decay of τ_2 :

$$\Delta T = \frac{\Delta T_{\max}}{2} \left[\text{erf} \left(\frac{t - t_0}{\tau_1 \sqrt{2}} \right) + 1 \right] \exp \left(-\frac{t - t_0}{\tau_2} \right) \quad (3)$$

Time constants τ_1 and τ_2 are only related to physical quantities, for example, a carrier cascade and relaxation time, but are not a direct measure of them (Supplementary Section 3). The edge positions t_0 are retrieved for each frequency $\Delta_i = \omega_i - \omega_0$ using equation (3) with variable parameters. We fit their curvature with a polynomial centred at $\omega_0 = 2\pi c/\lambda_0$:

$$t_0(\Delta) = p_1 + p_2 \Delta + p_3 \Delta^2 + \dots \quad (4)$$

This is similar to determining the first-order conditional moment with respect to frequency, which, in general, corresponds to the first derivative of the frequency-domain phase for a spectrogram²⁴. Because our spectrogram is gated in the time domain, we obtain an approximation of the spectral phase by fitting the edge positions $t_0(\Delta)$. Only the linear spectral phase can shift the temporal pulse envelope, so we identify the group delay φ_1 of the optical pulse as the constant term p_1 plus an unknown offset τ_0 to the

exact X-ray arrival time:

$$\varphi_1 = p_1 + \tau_0 \quad (5)$$

The term τ_0 accounts for the error of approximating the group delay with the constant p_1 and is constant from shot to shot if the spectral phase is stable. Rewriting $E(t)$ in the spectral domain with the Taylor expansion of the spectral phase around ω_0 (Supplementary Section 1) allows us to apply group delay to the optical pulse in the spectrogram:

$$\begin{aligned} S(\tau + p_1 + \tau_0, \tilde{\omega}) &= \left| \int dt G(t - \tau) \exp(i\tilde{\omega}t) E(t - p_1 - \tau_0) \right|^2 \\ &= \left| \int dt' G(t' - \tau + p_1 + \tau_0) \exp(i\tilde{\omega}t') E(t') \right|^2 \end{aligned} \quad (6)$$

With the transformation $t' = t - p_1 - \tau_0$ and dropping the phase factor $\exp(i\tilde{\omega}(p_1 + \tau_0))$, we find that a time shift of the gate function is equivalent to a shift in the opposite direction to the optical pulse; both result in a shift of the spectrogram. The relative time difference Δt of spectrogram S with arrival time $p_1 + \tau_0$ and S' with $p'_1 + \tau_0$ then depends only on the constant fitting parameters:

$$\Delta t = (p_1 + \tau_0) - (p'_1 + \tau_0) = p_1 - p'_1 \quad (7)$$

In the frame of the optical pulse, Δt is the difference in relative arrival times of two X-ray shots. The uncertainty of p_1 is given as the standard deviation from the least-squares fitting routine of the polynomial in equation (4).

We measured spectrograms that resulted from 800 eV X-ray pulses at the soft X-ray branch of the LCLS. We fit the model function (3) to each wavelength, as shown for a particular lineout in Fig. 2a. Fitting returns an r.m.s. error in t_0 for all lineouts from a particular X-ray shot, as shown in Fig. 2b. The error increases towards

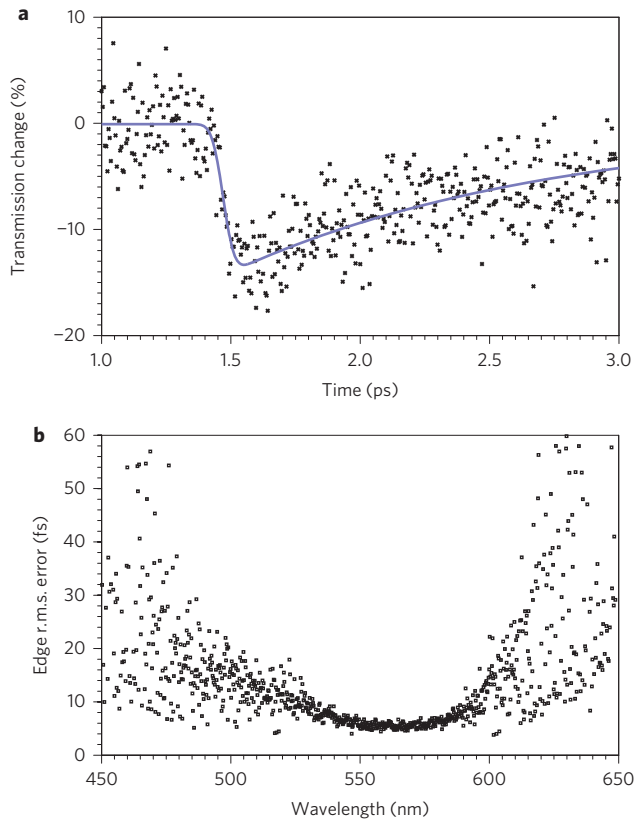


Figure 2 | Edge finding. **a**, Fitting of the transmission model (blue) to a lineout of the measured spectrogram (black). **b**, Error (r.m.s.) of edge position t_0 based on least-squares fitting of equation (3) for a single 110 μJ X-ray shot with 800 eV photon energy.

either side of the spectrum where noise begins to dominate the signal. The ~ 150 nm full-width at half-maximum (FWHM) of the bandwidth divided by our 1 nm spectrometer resolution provides us with effectively 150 independent edge positions.

This number of independent measurements can be scaled via the continuum bandwidth for more precise measurements of the X-ray arrival time. The r.m.s. error at each wavelength lineout is then used for a weighted fit of the polynomial in equation (4) and is calculated for each individual X-ray shot. We fit third-order polynomials because the spectral phase of our broadband continuum was dominated by terms of up to fourth order. Figure 3a presents a histogram of the r.m.s. error for the extracted relative arrival time p_1 based on 1,310 X-ray shots with pulse energies higher than 40 μJ . Nearly half of these shots have an r.m.s. error smaller than 1 fs. Figure 3b shows that there are diminished gains in signal amplitude at the 0.5 J cm^{-2} fluence level. Based on Fig. 3b we extract the fluence dependence of the transmission signal ΔT_{\max} up to a fluence F of 0.5 J cm^{-2} , where we observe the onset of saturation:

$$\Delta T_{\max} = F \times (0.369 \pm 0.004) \text{ cm}^2 \text{ J}^{-1} \quad (8)$$

To estimate how the numerical fitting error relates to the actual timing precision we need to investigate several additional effects. Given the long optical transport system at LCLS, we must address the concern about beam pointing. The geometry of the beam paths (Fig. 1) shows that movement along the respective pulse fronts, that is, a change in X-ray/optical offset, does not influence the timing precision. However, a change in angle affects the time-to-space mapping according to equation (1). Assuming an angle change of 20 μrad caused by airflow, vibration or mechanical

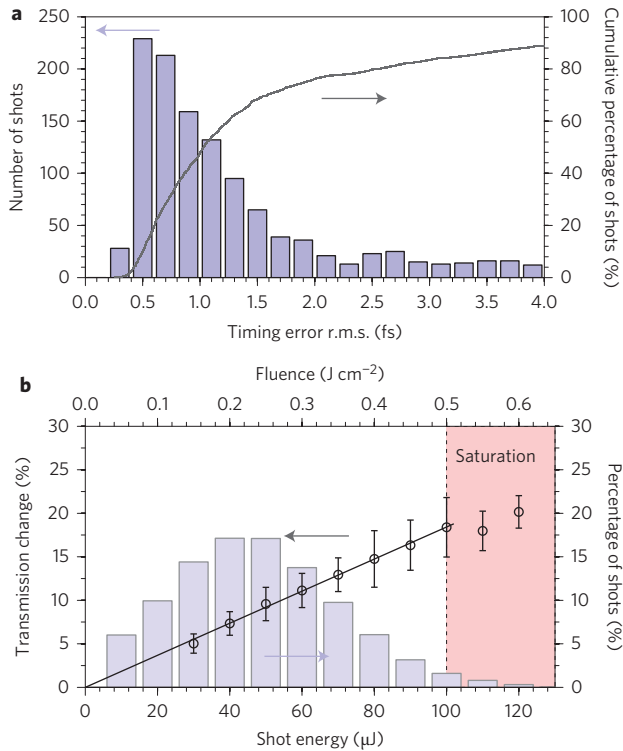


Figure 3 | Results for timing precision. **a**, Timing precision based on 1,310 shots with X-ray pulse energies greater than 40 μJ . Of the shots, 48% have an r.m.s. timing error below 1 fs. **b**, Scaling of transmission signals with X-ray fluence. The data points correspond to the left abscissa and the error bars are given as standard deviation. The induced transmission change increases linearly up to a fluence of 0.5 J cm^{-2} . Black line: fit of the linear regime with the slope given in equation (8).

instability of the optical mounts changes the time mapping by 0.004% or, equivalently, the time per pixel calibration by a negligible amount of 17 as. The power stability of the regeneratively amplified Ti:sapphire laser system may influence the spectral bandwidth and phase of the broadband continuum generated by filamentation in argon. However, spectral phase instabilities for this particular continuum generation scheme have been observed neither in the literature²⁵ nor with our separate online single-shot PG-XFROG²⁶ diagnostic (Supplementary Section 2). To be viable as a timing diagnostic, the timing jitter between the laser used for an experiment and the one used for timing should be stable to the desired precision, and preferably derived from the same source with minimal independent propagation (Supplementary Section 4). The feasibility for different photon energies is discussed in Supplementary Section 5.

In conclusion, we have demonstrated a new scheme for measuring the relative X-ray arrival time based on the single-shot measurement of an X-ray-induced, carrier-gated spectrogram with a broadband continuum pulse. Typical sources of error are suppressed, allowing for improved robustness and stability compared to other timing schemes routinely used at LCLS. This scheme presents a sub-femtosecond precision timing diagnostic for operation near 0.5 J cm^{-2} at 800 eV photon energy and may open a new avenue to measure time of arrival on the attosecond timescale.

Methods

Optical set-up. The experiment was carried out in the AMO Hutch of LCLS. A regeneratively amplified Ti:sapphire laser system delivered 30 fs pulses at 800 nm with a repetition rate of 120 Hz and pulse energy of 3 mJ, of which only $\sim 300 \mu\text{J}$ were used for continuum generation. The $\sim 1 \text{ cm } 1/e^2$ -diameter infrared beam was focused with a 1 m focal length lens into a 225 psi pressurized argon cell and thus

generated a supercontinuum via pulse filamentation²⁷. The incident intensity was finely adjusted to ensure single filament generation, and the resulting continuum was recollimated with a mirror with a 150 cm radius of curvature. The initial spectrum was more than 500 nm broad, but the optics in the set-up were chosen to reduce the optical bandwidth to ~150 nm FWHM. Dispersion compensation was achieved with a combination of grating and prism compressors, allowing independent control of second- and third-order dispersion, precompensating for material between the compressor and experimental chamber. The grating compressor consisted of a pair of 150 l/mm⁻¹ ruled gratings separated by ~20 cm. Blazed for 600 nm reflection, the gratings suppressed light below 400 nm. The prism compressor consisted of two equilateral BK7 prisms separated by ~1 m. Due to both the reduced bandwidth and the residual higher-order dispersion, the pulse width was 50 fs (r.m.s.). We estimate the temporal resolution of a single lineout as $t_{\text{res}} \approx \sqrt{\tau_{\text{FL}} \times \tau_{\text{chirped}}} = 12 \text{ fs}$, where τ_{FL} is the Fourier-limited pulse duration and τ_{chirped} is the measured pulse duration. This is sufficient temporal resolution for the measurement of the X-ray-induced signal. After compression, the continuum light was split into two beams using a Wollaston prism polarizer. A waveplate upstream of the Wollaston was adjusted for a 50/50 splitting ratio between the X-ray transmission measurement and a separate polarization-gated, cross-correlation, frequency-resolved optical gating (PG-XFROG) set-up with matched dispersion for independent online pulse characterization.

Detector calibration. The spectral window of the imaging spectrometer is 200 nm and was able to capture the full probe spectrum because of the reduced probe bandwidth. We used a Princeton Research Acton SP2500 with an Adimec OPAL 1000 nm camera. Images were recorded at 120 Hz, with every 11th X-ray shot dropped to serve as an unpumped normalization spectrogram. The 1,024 × 1,024 pixels of the camera were measured to have a wavelength calibration of 0.217 nm per pixel along the horizontal and 4.5 fs per pixel along the vertical.

Beam parameters. The optical beam was astigmatically focused on a 500-nm-thick silicon nitride membrane, resulting in an estimated 1.3 mm × 30 μm line focus. The FEL was operated in low-charge mode with a slotted spoiler generating X-ray pulses of ~3 fs duration and an average pulse energy of 47 μJ. The photon energy of 800 eV corresponds to an attenuation length of 0.7 μm in silicon nitride. With the sample surface oriented normal to the optical probe propagation vector, the effective thickness for the 45° angle of incidence of the X-ray beam was 0.5 μm × √2 ≈ 0.7 μm, thereby depositing (1 - 1/e) ≈ 63% of the X-ray pulse energy in the sample. The X-ray beam was overlapped with the line focus of the optical probe onto the sample membrane, with a full-width beam size of 20 ± 5 μm by 700 ± 25 μm estimated by high-resolution microscopic inspection of damage spots on the sample holder. This led to an underestimate of the transmission signals because the optical beam overfilled the X-ray spot, and only part of the probe beam experienced the change in transmission.

Received 13 November 2013; accepted 19 June 2014;
published online 27 July 2014

References

- Ding, Y. *et al.* Femtosecond X-ray pulse characterization in free-electron lasers using a cross-correlation technique. *Phys. Rev. Lett.* **109**, 254802 (2012).
- Fritz, D. M. *et al.* Ultrafast bond softening in bismuth: mapping a solid's interatomic potential with X-rays. *Science* **315**, 633–636 (2007).
- Glownia, J. M. *et al.* Time-resolved pump–probe experiments at the LCLS. *Opt. Express* **18**, 17620–17630 (2010).
- Sato, T. *et al.* Development of ultrafast pump and probe experimental system at SACLA. *J. Phys. Conf. Ser.* **425**, 092009 (2013).
- Ding, Y. *et al.* Femtosecond X-ray pulse temporal characterization in free-electron lasers using a transverse deflector. *Phys. Rev. ST Accel. Beams* **14**, 120701 (2011).
- Grgurăš, I. *et al.* Ultrafast X-ray pulse characterization at free-electron lasers. *Nature Photon.* **6**, 852–857 (2012).
- Hoffmann, M. C. & Turner, J. J. Ultrafast X-ray experiments using terahertz excitation. *Synchrotron Radiat. News* **25**, 17–24 (2012).
- Cunovic, S. *et al.* Time-to-space mapping in a gas medium for the temporal characterization of vacuum-ultraviolet pulses. *Appl. Phys. Lett.* **90**, 121112 (2007).
- Bionta, M. R. *et al.* Spectral encoding of X-ray/optical relative delay. *Opt. Express* **19**, 21855–21865 (2011).
- Schorb, S. *et al.* X-ray-optical cross-correlator for gas-phase experiments at the Linac Coherent Light Source free-electron laser. *Appl. Phys. Lett.* **100**, 121107 (2012).
- Krupin, O. *et al.* Temporal cross-correlation of X-ray free electron and optical lasers using soft X-ray pulse induced transient reflectivity. *Opt. Express* **20**, 11396–11406 (2012).
- Harmand, M. *et al.* Achieving few-femtosecond time-sorting at hard X-ray free-electron lasers. *Nature Photon.* **7**, 215–218 (2013).
- Riedel, R. *et al.* Single-shot pulse duration monitor for extreme ultraviolet and X-ray free-electron lasers. *Nature Commun.* **4**, 1731 (2013).
- Mukamel, S., Healion, D., Zhang, Y. & Biggs, J. D. Multidimensional attosecond resonant X-ray spectroscopy of molecules: lessons from the optical regime. *Annu. Rev. Phys. Chem.* **64**, 101–127 (2013).
- Biggs, J. D., Zhang, Y., Healion, D. & Mukamel, S. Two-dimensional stimulated resonance Raman spectroscopy of molecules with broadband X-ray pulses. *J. Chem. Phys.* **136**, 174117 (2012).
- Gahl, C. *et al.* A femtosecond X-ray/optical cross-correlator. *Nature Photon.* **2**, 165–169 (2008).
- Beye, M. *et al.* X-ray pulse preserving single-shot optical cross-correlation method for improved experimental temporal resolution. *Appl. Phys. Lett.* **100**, 121108 (2012).
- Sokolowski-Tinten, K., Cavalleri, A. & von der Linde, D. Single-pulse time- and fluence-resolved optical measurements at femtosecond excited surfaces. *Appl. Phys. A* **69**, 577–579 (1999).
- Bionta, M. R. *et al.* Spectral encoding based measurement of X-ray/optical relative delay to ~10 fs rms. *Proc. SPIE* **8504**, 85040M (2012).
- Kane, D. J. & Trebino, R. Characterization of arbitrary femtosecond pulses using frequency-resolved optical gating. *IEEE J. Quantum Electron.* **29**, 571–579 (1993).
- Ziaja, B., London, R. A. & Hajdu, J. Unified model of secondary electron cascades in diamond. *J. Appl. Phys.* **97**, 064905 (2005).
- Medvedev, N., Jeschke, H. O. & Ziaja, B. Nonthermal phase transitions in semiconductors induced by a femtosecond extreme ultraviolet laser pulse. *New J. Phys.* **15**, 015016 (2013).
- Sundaram, S. K. & Mazur, E. Inducing and probing non-thermal transitions in semiconductors using femtosecond laser pulses. *Nature Mater.* **1**, 217–224 (2002).
- Cohen, L. Time-frequency distributions—a review. *Proc. IEEE* **77**, 941–981 (1989).
- Gu, X. *et al.* Generation of carrier-envelope-phase-stable 2-cycle 740-μJ pulses at 2.1-μm carrier wavelength. *Opt. Express* **17**, 62–69 (2009).
- Linden, S., Giessen, H. & Kuhl, J. XFROG—a new method for amplitude and phase characterization of weak ultrashort pulses. *Phys. Status Solidi B* **206**, 119–124 (1998).
- Hauri, C. P. *et al.* Generation of intense, carrier-envelope phase-locked few-cycle laser pulses through filamentation. *Appl. Phys. B* **79**, 673–677 (2004).

Acknowledgements

The authors thank S. Durbin, D. Reis, A. Lindahl and R. Schoenlein for discussions of bulk material X-ray interactions. W.H. acknowledges financial support from a Marie Curie fellowship. T.F. acknowledges financial support from National Center of Competence in Research, Molecular Ultrafast Science and Technology. This research was carried out at the Linac Coherent Light Source (LCLS) at the SLAC National Accelerator Laboratory. LCLS is an Office of Science User Facility operated for the US Department of Energy Office of Science by Stanford University.

Author contributions

N.H. and R.N.C. conceived and coordinated the experiment. M.R.B., J.G. and R.N.C. carried out sample preparation. N.H., W.H., A.G., J.M.G., D.J.K. and R.N.C. built the optical set-up. M.R.B., K.R.E., S.S., M.J.S., S.C., C.B., J.-C.C. and J.B. carried out instrument control and integration. N.H. and D.J.K. performed data analysis. N.H., R.N.C., T.F., C.P.H. and W.H. interpreted data. R.N.C., T.F., C.P.H., A.R.F., W.E.W. and S.L.M. oversaw manuscript production. N.H. wrote the paper with extensive suggestions from R.N.C., T.F., C.P.H., W.H. and D.J.K. and contributions from all other authors.

Additional information

Supplementary information is available in the online version of the paper. Reprints and permissions information is available online at www.nature.com/reprints. Correspondence and requests for materials should be addressed to N.H. and R.N.C.

Competing financial interests

D.J.K., head of Mesa Photonics, has referenced some of the results herein for SBIR proposals regarding the development of temporal X-ray diagnostics.